2014 IEEE International Conference on Robotics & Automation (ICRA)
Hong Kong Convention and Exhibition Center
May 31 - June 7, 2014. Hong Kong, China

Design of a Teleoperated Robotic System for Retinal Surgery

A. Gijbels, E.B. Vander Poorten, P. Stalmans, H. Van Brussel, D. Reynaerts

***Abstract*— Retinal surgery is one of the most challenging types of surgery because of the scale and the fragility of the human eye anatomy. The surgeon suffers from limited positioning accuracy, tremor and poor force feedback directly affecting the quality of the surgical procedures. To tackle these issues, we developed a teleoperation system to assist surgeons during retinal surgery. The system offers features like motion scaling, tremor compensation and scaled force feedback. This paper reports on the design of the slave and the master.**

I. Introduction

During retinal surgery, the surgeon performs procedures at the retina. Figure 1 conceptually illustrates the surgical scene inside the eye. Retinal surgery is a type of Minimally Invasive Surgery (MIS). Small incisions are made in the sclera and equipped with trocars. The surgeon manually guides the surgical instruments through the trocars and avoids moving these trocars as much as possible in order to keep the eye steady and to prevent excessive forces on the sclera. This limits the degrees of freedom (DOFs) at the incision point to three rotations θ, ϕ and ψ and a translation R. In some cases the instrument consists of a gripper which can be considered as a fifth DOF. The surgeon uses a stereoscopic microscope placed just above the patient's eye lens to get visual feedback on the surgical scene (see Fig. 2). Because of the presence of the microscope the surgeon can only move the instruments in a very confined space. The surgeon manipulates the instruments while placing his/her hands on the patient's forehead minimizing the force loop and therefore resulting in the highest achievable positioning precision. Still, retinal surgery is considered as one of the most challenging types of surgery because of the scale and the fragility of the retinal anatomy. Retinal tissue can be as thin as 25 µm and retinal vessels can have a diameter as small as 10 µm. Riviere et al. [1] showed that the surgeon suffers from physiological tremor with an rms amplitude of 182 µm. Gupta et al. [2] showed that 75% of the interaction forces between the instrument and the retina are lower than 7.5 mN. The surgeon can only feel these forces in 19% of the cases explaining why the surgeon can rely solely on visual feedback. These limitations directly affect the quality of these difficult procedures [2]. For some envisioned treatment methods, it is even impossible to safely perform the necessary manipulations leaving the surgeon to rely on less effective treatment methods.

Andy Gijbels, Emmanuel Benjamin Vander Poorten, H. Van Brussel and Dominiek Reynaerts are with the Department of Mechanical Engineering, University of Leuven, 3001 Heverlee, Belgium

Peter Stalmans is with the Department of Ophthalmology, University of Leuven, 3000 Leuven, Belgium

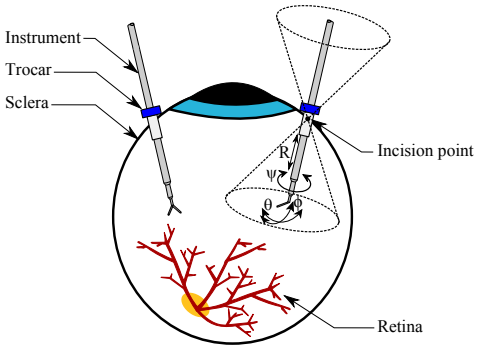

Fig. 1. Retinal surgeons generally use 4 DOFs to manoeuvre instruments inside the eye: three rotations θ, ϕ and ψ around the incision point and a translation R through the incision point. Translational movements tangential to the eye ball are avoided since these movements rotate the eye, complicating targeting, and can result in excessive forces on the sclera.

Fig. 2. Left: Surgical scene during a retinal procedure. Right: The surgeon needs to operate in a highly confined space due to the presence of the microscope and a spherical lens. The spherical lens is used to get a large viewing angle inside the eye without the necessity to rotate the eye during the procedure.

A fair number of robotic systems for retinal surgery have been reported in literature to address the abovementioned issues. Riviere's group at Carnegie Mellon University developed a hand-held device capable of limited motion scaling and actively reducing tremor [3]. Taylor's group at Johns Hopkins University firstly introduced a co-manipulation technique for retinal surgery [4]. Here, the surgeon shares control over the instrument with a robotic arm. The robotic arm successfully filters all noticeable tremor and limits the speed of the instrument in order to obtain a higher positioning accuracy. The same group also does research on the development of force sensors which can be integrated in the surgical tool. The use of these force sensors enables the implementation of force-based virtual fixtures and auditive feedback on the level of forces applied by the surgeon. Steinbuch's group at TUEindhoven developed a teleoperation system

978-1-4799-3684-7/14/$31.00 ©2014 IEEE

consisting of a custom-made haptic master controlling the movements of custom-made slave. Benefits of such a system like motion scaling, tremor compensation and scaled force feedback motivate their work [5]. Other robotic systems designed for retinal surgery are described in [6]–[9].

Previously, the authors developed a surgical manipulator to assist surgeons during retinal procedures using the co-manipulation technique [10], [11]. Within the scope of the same research project, this system was extended towards a teleoperation system to explore possible additional benefits like motion scaling, scaled force feedback and better ergonomics and to validate whether these advantages truly outweigh the additional complexity of such system. This paper reports on the design of the slave and the master which form this newly designed teleoperation system. Section II briefly discusses the most important design requirements of the teleoperation system. Section III and IV discuss the design of the slave and the master respectively. Section V presents the realised system.

II. Design requirements

In interaction with several microsurgeons a non-exhaustive list of design requirements was compiled. The most fundamental requirements are described below.

The targeted procedures are retinal vessel cannulation and epiretinal membrane peeling, since it is extremely difficult to perform these treatments adequately. During a retinal vessel cannulation, a needle needs to be inserted into a retinal vessel with a diameter as small as 10 µm in order to inject a fluid. During epiretinal membrane peeling, the surgeon's goal is to remove scar tissue located on top of the retina with an approximate thickness of 25 µm. The surgeon requires an available workspace on the retina of 60° around the center of the eye to perform these delicate procedures. To provide sufficient manipulation freedom, this area is increased to 90° (see Fig. 3). In order to reach the retina with his/her instruments, the surgeon creates an incision at approximately 4 mm from the corneal limbus. No vital tissue is present at this location. Considering this data and taking into account the variety of the human eye anatomy [12], ranges for the desirable DOFs are derived and summarized in Table I. A positioning precision of 3 µm at the tip of the instrument is sufficient to safely manipulate the thinnest retinal tissue and the smallest retinal vessels. From this target value, the desirable precision for the different DOFs is calculated (Table I). Consideration of instruments with a curved tip and their intended application leads to a desirable precision of 1° for the ψ-DOF. Based on experiments, forces at the control handle of the master up to 10 N in the R-, θ- and ϕ-DOF and a torque in the ψ-DOF up to 50 mNm are considered to be useful for high fidelity force feedback. Initially, a possible fifth DOF, incorporated in the instrument, is not considered since this DOF is not necessarily required in order to perform the envisioned procedures.

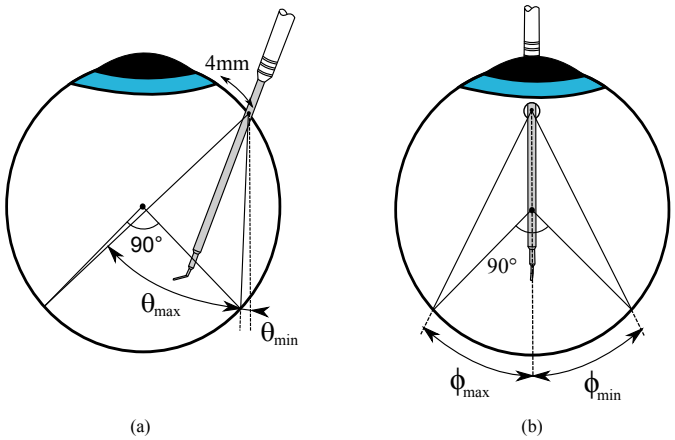

Fig. 3. Left: required work range in θ. Right: required work range in ϕ.

TABLE I
Design requirements for the different DOFs

	Tip	R	θ	ϕ	ψ
Range		30 mm	$+50°$	$\pm 28°$	$+360°$
Precision	3 µm	3 µm	$0,007°$	$0,007°$	$0,3°$
Forces		10 N	10 N	10 N	50 mNm

III. The Slave

As mentioned earlier, the authors already developed a robotic manipulator for assistance during retinal surgery using a co-manipulation technique. This robotic manipulator complies with all stated design requirements, except for the ψ-DOF which was designed to be passive for this shared-control technique. To solve this issue, an active ψ-module was designed and integrated in the system. Also the $R\theta$-drive mechanism was redesigned and updated. The new robotic manipulator is suited to be used as the slave in the intended teleoperation system. The derivation of the kinematic structure and the associated kinematic equations and workspace are detailed in [11]. This section briefly resumes the outline of the kinematic structure and discusses the updated design of the slave.

A. Kinematics of the slave mechanism

As mentioned earlier, only 4 DOFs (R,θ, ϕ and ψ) are required at the incision during retinal surgery. The slave implements these DOFs at a point distal from its mechanical components. In this way, the area around the incision point is kept unoccupied when both points are pre-operatively aligned. Such a point is called a Remote Center of Motion (RCM) and can be implemented using an RCM mechanism. A handful of substantially different RCM mechanisms have been reported in literature [13]. None of the earlier designs appeared to be really suited to be incorporated in the slave since they all realise the R-DOF by adding a linear drive mechanism at the end-effector. Considering the tight space constraints associated with retinal procedures as discussed earlier, such a voluminous end-effector is not desirable.

Therefore a novel 4 DOF RCM mechanism, depicted in Fig. 4, that implements the R-DOF at the base of the mechanism was designed. The mechanism can tilt around the ϕ-axis. The R- and θ-movements are implemented using a multi-parallelogram bar mechanism. The prismatic joint at the base of the mechanism allows remote actuation of the insertion and retraction motion and thus helps keeping the end-effector more compact. Figure 5 demonstrates the working principle for actuating the θ- and R-movement respectively. The ψ-DOF is implemented at the end-effector since this can be done in a compact way as detailed later on. The ϕ- and ψ-DOF are controlled independently using joints q_1 and q_4 respectively. The R- and θ-DOF are controlled simultaneoulsy by using joints q_2 and q_3.

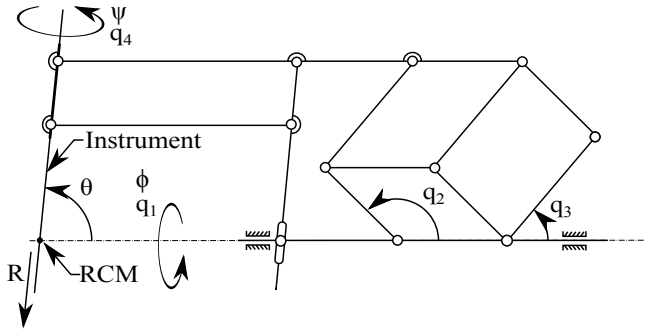

Fig. 4. The slave consists of a novel RCM mechanism implementing 4 DOF R,θ, ϕ and ψ which are driven by joints q_1, q_2, q_3 and q_4.

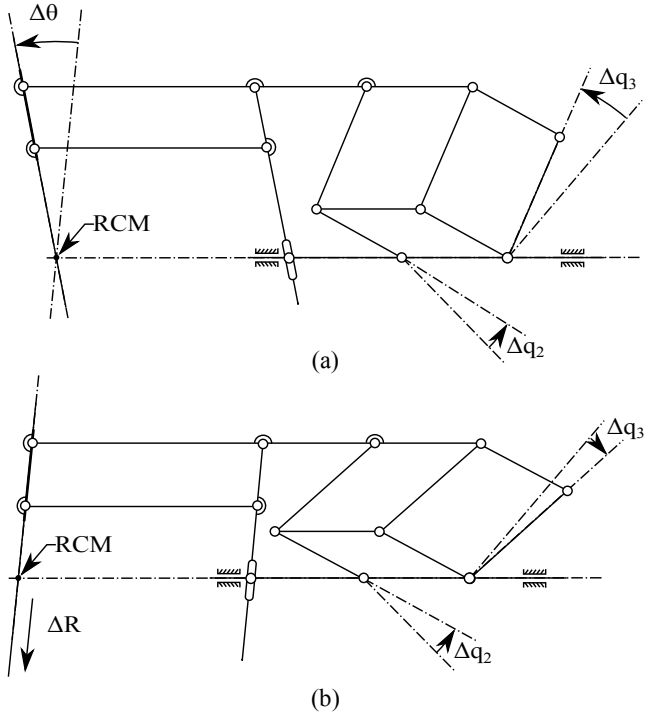

Fig. 5. Demonstration of the θ- (a) and R-movement (b) of the $R\theta$-mechanism through coordinated control of the q_2 and q_3 joints.

B. Design details of the slave

Figure 6 depicts a perspective view on the final design of the slave. Nearly all moving components are mounted on top of a base. This base can turn around the ϕ-axis with respect to the support structure. The linkages of the $R\theta$-mechanism are H-shaped and fit into one another to prevent collisions inside the intended workspace. The system is almost perfectly symmetric with respect to a plane through ϕ-axis and perpendicular to the base. Counterweights are attached to both the q_2- and the q_3-linkage. Thanks to these design considerations, gravitational effects on the slave are negligible with respect to the torque characteristics of the different drive mechanisms. Joints q_1, q_2 and q_3 are driven by capstan drive mechanisms to avoid backlash and limit friction. Figure 7 shows the arrangement of these drive mechanisms. All three are actuated by a Maxon RE30 DC-motor. The capstan gear ratios are equal to 12:1, 10:1 and 10:1 respectively. To achieve the desired positioning accuracy at the tip of the needle, the q_1-motor is equipped with a GPI 65536 cpr (counts per revolution) encoder. The q_2- and q_3-drives both contain a GPI 144000 cpr encoder. Note that these encoders are directly attached to the q_2- and q_3-axis respectively. The ψ-module consists of a drive mechanism to rotate the instrument around its axis and an instrument clamping mechanism (see Fig. 8). The clamping mechanism comprises a collet washer and a collet which is screwed into a hollow shaft. Placing an instrument through the hollow shaft and manually rotating the washer with respect to the shaft will fix the instrument. The hollow shaft is driven by the q_4-drive mechanism. Here, the actuation is provided by a Maxon RE8 DC-motor equipped with a Maxon MR 100 CPT encoder and a 6:1 zero-backlash gear set. The overall dimensions of the slave are $27 \times 37 \times 20$ cm. The total mass of the moving parts is limited to 1.5 kg. Table II summarizes the range, accuracy, resolution and force/torque for the different DOFs of the slave. By comparing Table I and Table II it can be seen that all the design requirements are effectively met. Since the workspace shape of the $R\theta$-mechanism is non-polar, no general range can be defined for the R- and θ-DOF. Nevertheless, the workspace is sufficiently large to span the intended workspace on the retina [11].

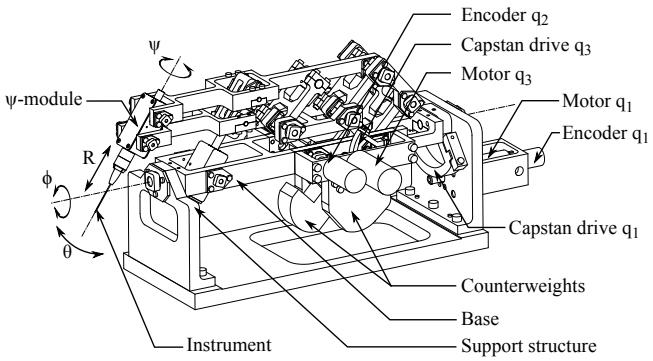

Fig. 6. Perspective view on the design of the slave.

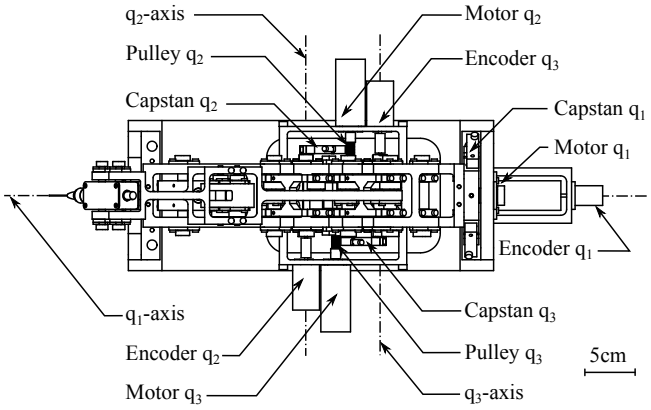

Fig. 7. Top view on the slave system design clarifying the layout of the q_1, q_2 and q_3 drive mechanisms.

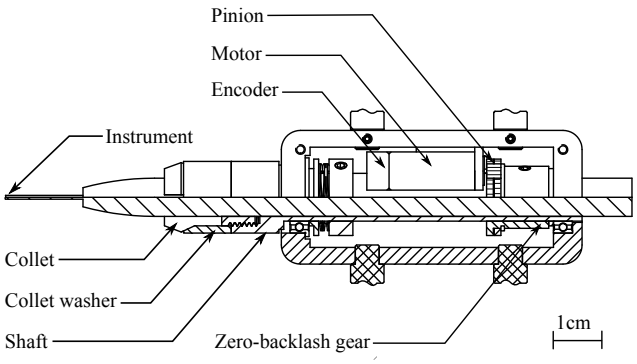

Fig. 8. View on the inside of the ψ-module. The lower part shows a cross-section view through the instrument axis. The mechanism consists of a ψ-drive mechanism and a collet clamping mechanism.

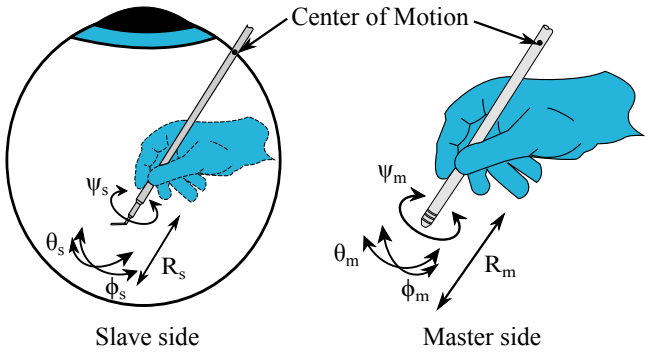

Fig. 9. The surgeon manipulates the master handle using spherical DOFs, typical to retinal surgery, in order to control the instrument's motion. The pose of the handle is directly mapped onto the pose of the instrument avoiding motion inversion.

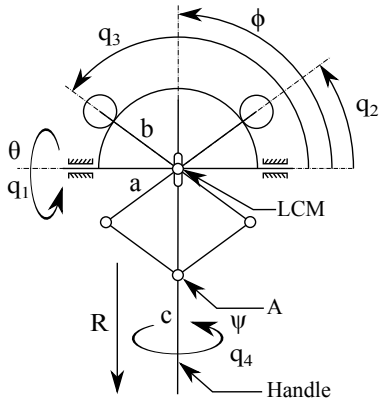

Fig. 10. The master is a spherical mechanism implementing 4 DOFs R, θ, ϕ and ψ at a Local Center of Motion. These DOFs are driven by joints q_1, q_2, q_3, q_4.

IV. The Master

Master devices used in teleoperation systems for MIS are typically designed for Cartesian control, mapping the motions of the master handle onto the tip of the surgical instrument, with or without additional local DOFs. In this way, dexterity loss due to problematic hand-eye coordination and motion inversion, typical to MIS but not present in conventional open surgery, can be alleviated. On the contrary, retinal surgeons are used to this MIS way of instrument manipulation and might even prefer it. This motivates the use of a spherical master in the intended teleoperation system. Such a spherical master can also compensate for motion inversion, like illustrated by Fig. 9. None of the commercially available haptic masters complies with the stated design requirements. Therefore a custom-made haptic master is developed. Since no previous work by the authors describes the development of this device, the design will be discussed here in greater detail.

TABLE II

Properties for the different DOFs of the slave.

	R	θ	ϕ	ψ
Range	ok [11]	ok [11]	$\pm 45°$	$\infty°$
Resolution	≤ 1 µm	$\leq 0{,}0002°$	$0{,}0007°$	$0{,}24°$
Cont. Force/ Torque	≥ 10 N	≥ 1 Nm	1 Nm	3,5 mNm

A. Kinematics of the master mechanism

The master consists of novel spherical mechanism able to move a handle in 4 DOFs R, θ, ϕ and ψ (see Fig. 10). The master implements these DOFs at a Local Center of Motion (LCM). The mechanism can tilt around the θ-axis. The R- and ϕ-movements are implemented using a parallelogram-based bar mechanism attached to the handle. The handle is supported by a revolute and prismatic joint at the LCM. Figure 11 demonstrates a ϕ- and R-movement of this mechanism respectively. The ψ-DOF is implemented locally at the handle. The θ- and ψ-DOF are controlled independently using joints q_1 and q_4 respectively. The R- and ϕ-DOF are controlled simultaneously using joints q_2 and q_3. The arc and the two circles tangent to this arc depicted in Fig. 10 represent two capstan drive mechanisms used to control joints q_2 and q_3 as will be discussed later on.

Given this actuation scheme the Jacobian $\mathbf{J}$, which maps the joint velocities $\dot{q}_1$, $\dot{q}_2$, $\dot{q}_3$ and $\dot{q}_4$ to the end-effector

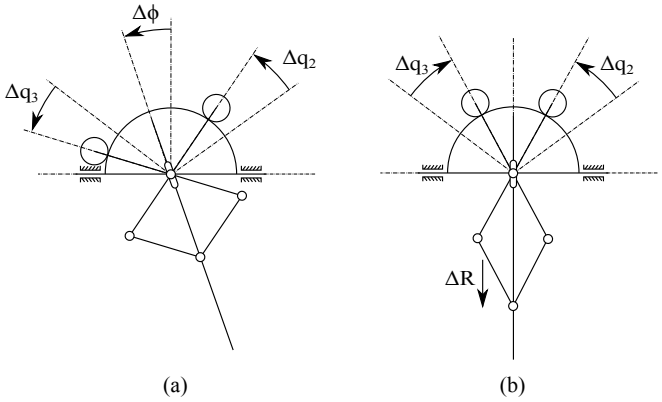

Fig. 11. Demonstration of the ϕ- (a) and R-movement (b) of the $R\phi$-mechanism through coordinated control of the q_2 and q_3 joints.

translational and rotational velocities $\dot{R}$, $\dot{\theta}$, $\dot{\phi}$ and $\dot{\psi}$, can be formulated as:

$$\begin{bmatrix} \dot{R} \\ \dot{\theta} \\ \dot{\phi} \\ \dot{\psi} \end{bmatrix} = \mathbf{J}(\mathbf{q}) \begin{bmatrix} \dot{q}_1 \\ \dot{q}_2 \\ \dot{q}_3 \\ \dot{q}_4 \end{bmatrix}, \text{ with } \mathbf{J}(\mathbf{q}) = \begin{bmatrix} 0 & -A & A & 0 \\ 1 & 0 & 0 & 0 \\ 0 & \frac{1}{2} & \frac{1}{2} & 0 \\ 0 & 0 & 0 & 1 \end{bmatrix} \quad (1)$$

and

$$A = \frac{a\sin(q_3 - q_2)}{\sqrt{2(1+\cos(q_3 - q_2)}}.$$

The parameter a represents the parallelogram linkage length. Solving the equation $det(\mathbf{J}(\mathbf{q})) = 0$, shows that the mechanism possesses singularities for $q_2 = q_3$ and for $q_2 = q_3 - \pi$. These singularities correspond to the configurations where two pair of consecutive linkages of the parallelogram are parallel.

The link length a is chosen to fit the workspace of the $R\phi$-mechanism to the kinematic requirements listed in Table I. Collisions between the mechanical components of the $R\phi$-mechanism, influencing the workspace, are taken into account. Multiple design iterations led to a link length $a =$ 51 mm. The resulting workspace boundaries are described by:

$$\begin{aligned} q_2 &\approx [15^\circ, 132^\circ], \\ q_3 &\approx [48^\circ, 165^\circ], \\ q_3 &\geq q_2 + 24^\circ. \end{aligned} \quad (2)$$

The resulting joint workspace for the $R\phi$-mechanism is shown in Fig. 12(a). The red line and the red dot indicate the singularities when $q_2 = q_3$ and $q_2 = q_3 - \pi$ respectively. These singularities clearly lie outside the workspace. $R\phi$-workspace is calculated using the forward kinematic equations (which will be referred to as FKE in the following). Since the $R\phi$-mechanism is a polar mechanism, similar conclusions regarding the workspace can be drawn using any reference point on the handle. For clarity of the resulting figure, point A on the handle is used as a reference point

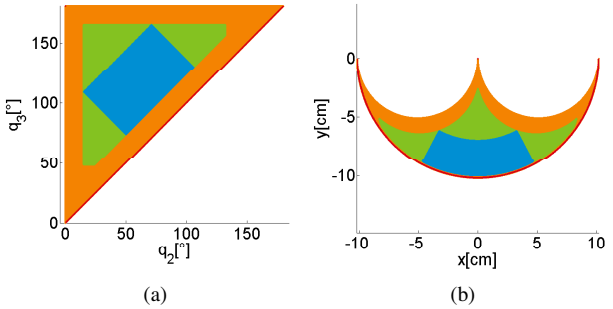

Fig. 12. The joint (left) and polar (right) workspace (green) of the $R\phi$-mechanism. The blue area represents the workspace requirement. The orange and green area represent the theoretical and actual workspace respectively. The red dot and line corresponds to the singular configurations.

(see Fig. 10). This leads to the following FKE:

$$\begin{aligned} R &= a\sqrt{2(1+\cos(q_3 - q_2))}, \\ \theta &= q_1 \\ \phi &= \frac{q_2 + q_3}{2}, \\ \psi &= q_4. \end{aligned} \quad (3)$$

Figure 12 shows the resulting $R\phi$-workspace (green). The design requirement (blue) is clearly met. The extra space the workspace offers is useful when a scaling factor between the master and slave motions is applied.

B. Design details of the master

Figure 13 depicts a perspective view on the final design of the master. The $R\theta\phi\psi$-mechanism is rigidly attached to a back plate elevating the system with respect to a hand support plate. In this way, it is possible to freely move the handle inside the intended workspace while avoiding any collision between the surgeon's hand and the device. The $R\phi\psi$-module can rotate around the θ-axis with respect to the mechanism support structure. This DOF is driven by a capstan drive mechanism to avoid backlash and limit friction. The drive consists of a Maxon RE30 DC-motor equipped with a Scancon 7500 cpr encoder which remains stationary with respect to the support structure. The capstan gear ratio is equal to 26:1. The the $R\phi\psi$-module is covered, protecting its components from being damaged. The handle has a length of 100 mm and a diameter of 10 mm. These dimensions are comparable to those of a surgical tool.

Figure 14 shows the design of the $R\phi$-module. For clarity, the ψ-module is made invisible in this figure. The linkages of the parallelogram are angled to maximise the available workspace while keeping the mechanism as compact as possible. The θ-,ϕ- and ψ-axis intersect in the LCM. The prismatic joint at the LCM is implemented by virtue of a ball spline. The use of a ball spline rather than a conventional linear bushing is motivated later on. Joints q_2 and q_3 are driven by two seperate capstan drive mechanisms in order to move the parallelogram structure. Each drive consists of a Maxon RE30 DC-motor equipped with a Scancon 7500

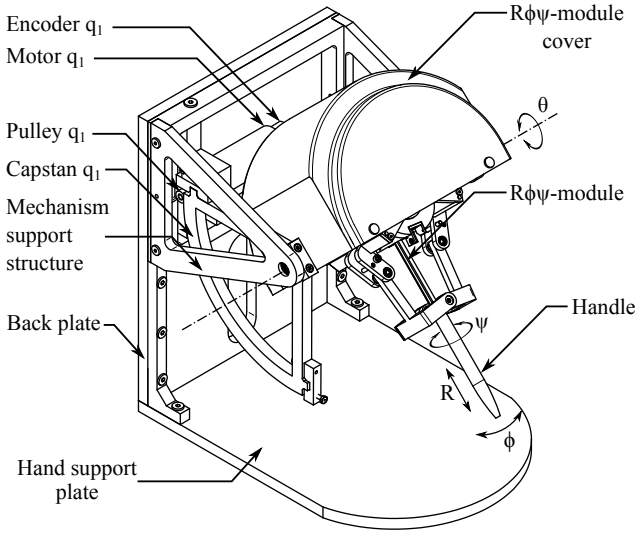

Fig. 13. Overview on the design of the haptic master and detailed design of the q_1 capstan drive mechanism. For clarity, the $R\phi\psi$-module is (partially) covered in this figure.

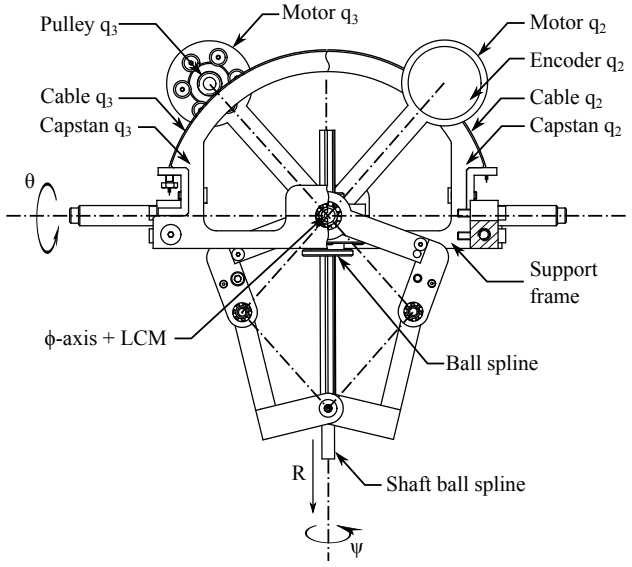

Fig. 14. Detailed design of the $R\phi$-module. For clarity, the ψ-module is made invisble in this figure. The right part of this figure shows a broken-out section view behind the capstan of joint q_3.

cpr encoder. The capstan gear ratios are both equal to 13:1. Unlike the capstan drive mechanism of joint q_1, these capstans remain stationary while the motors are moving with respect to these capstans.

Figure 15 shows the design of the ψ-module. The module is designed in such a way that the q_4 drive mechanism remains stationary with respect to the support frame of the $R\phi$-module. This is done using a ball spline able to transmit torque to the shaft while still allowing translation. Joint q_4 consists of a capstan drive mechanism. The drive is actuated through a Maxon EC 20 flat equipped with a Baumer 1025 cpr Magnetic Encoder. The motor and encoder support is

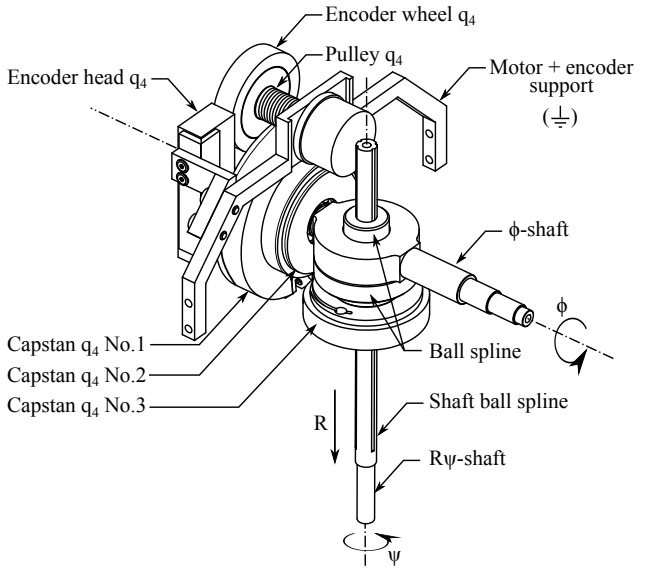

Fig. 15. Detailed design of the ψ-module.

attached to the support frame of the $R\phi$-module. The capstan mechanism is composed out of three capstans. The motor pulley and Capstan No.1 are used to magnify the motor torque. The gear ratio of this capstan mechanism is equal to 5,4:1. Capstan No.2 and No.3 form a cable-based bevel transmission. This is done to prevent collisions between the q_4-capstan drive mechanism and the $R\phi$-module while keeping the total master as compact as possible.

The overall dimensions of the master are $27 \times 27 \times 20$ cm. Table II summarizes the range, accuracy, resolution and force/torque for the different DOFs of the master. By comparing Table I and Table III it can be seen that nearly all the design requirements are effectively met. The torque in the ψ-DOF forms an exception which is in fact very close to its specification of 50 mNm and the range of the ψ-DOF is limited to 210° because of the q_4 capstan drive mechanism. The latter forms no problem since the master can momentarily be decoupled from the slave and repositioned when this workspace limit is met.

TABLE III
PROPERTIES FOR THE DIFFERENT DOFS OF THE MASTER.

	R	θ	ϕ	ψ
Range	ok Fig.12(b)	90°	ok Fig.12(b)	210°
Resolution	≤ 1.5 μm	$\leq 9\mu^\circ$	$\leq 16\mu^\circ$	$\leq 0,24^\circ$
Cont. Force/ Torque	≥ 22 N	≥ 11 N	≥ 11 N	44 mNm

V. REALISATION OF THE TELEOPERATION SYSTEM

Figure 16 shows the realised teleoperation setup. Both master and slave have been fabricated. Next to the master and the

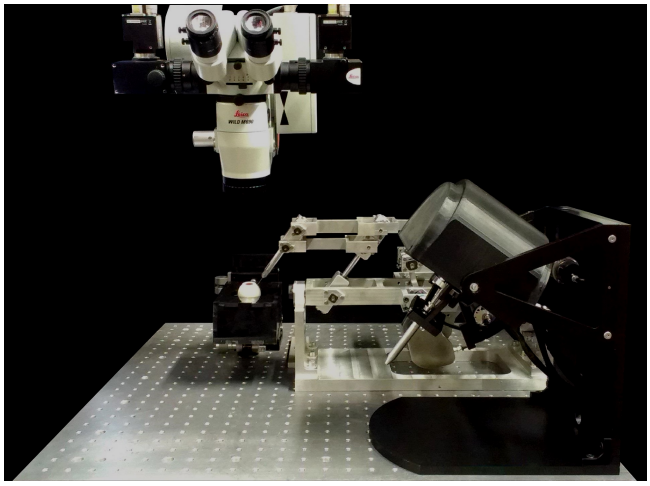

Fig. 16. Experimental setup consisting of the master, the slave, a stereoscopic microscope and a custom-made mock-up of the human eye.

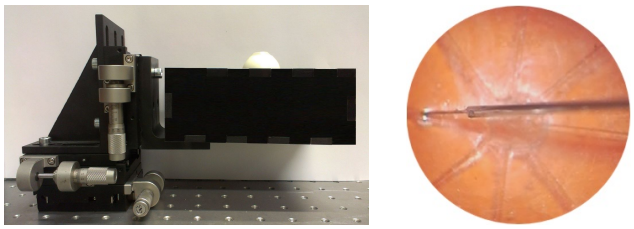

(a) (b)

Fig. 17. An artificial eye (left) with a polymer retina (right) is placed into a gimbal mechanism simulating the human eye and its natural rotational DOFs. The mechanism is covered by the black box. The system is attached to an XYZ-platform in order to align the incision point in the eye with the RCM of the slave.

slave, the setup contains a stereoscopic microscope and a mockup of a human eye. Figure 17 depicts the eye mockup. The eye is inserted into a cardan-like mechanism in order to simulate the natural rotational DOFs of a human eye. A custom-made artificial retina is made and placed inside the eye to enable the simulation of some of the most challenging retinal procedures in a non-clinical environment. In order to align the RCM of the slave with the incision in the eye, the eye mockup is mounted upon a XYZ-platform. Preliminary control schemes already have been implemented in the teleoperation system. Video recordings in attachment to this paper demonstrate the RCM of the slave and features like tremor compensation and motion scaling between the master and the slave.

VI. Conclusion and Future work

This work reported on the development of a teleoperation system to assist retinal surgeons during the most delicate procedures. The system enables motion scaling, tremor compensation, the implementation of active constraints or scaled force feedback. For this purpose a slave and master were designed. The slave device consists of an innovative 4DOF RCM mechanism kinematically constraining the incision point to prevent unwanted eye motions and excessive force on the sclera. The slave is controlled using a 4DOF spherical master. The device is active in all its DOFs enabling the implementation of active constraints and scaled force feedback of the interaction forces between the retinal tissue and the instrument. Both the master and the slave have been successfully fabricated. Currently, the authors are working on the development of force sensors which can be integrated in the surgical tool. Experiments with scaled force feedback will follow in the future.

VII. Acknowledgments

This work was supported by an FP7-People Marie Curie Reintegration Grant, PIRG03-2008-231045 and by a PhD grant from the Institute for the Promotion of Innovation through Science and Technology in Flanders (I.W.T.-Vlaanderen), 101445

References

[1] C. N. Riviere and P. S. Jensen, "A study of instrument motion in retinal microsurgery," *Proc. of the 22nd Annual EMBS Int. Conf.*, 2000.

[2] P. Gupta, P. Jensen, and E. Juan, "Surgical forces and tactile perception during retinal microsurgery," *Proc. of the Second Int. Conf. on Medical Image Computing and Computer Assisted Intervention (MICCAI)*, pp. 1218–1225, 1999.

[3] S. Yang, R. A. MacLachlan, and C. N. Riviere, "Design and analysis of 6 dof handheld micromanipulator," *Proc. IEEE Int. Conf. on Robotics and Automation (ICRA).*, pp. 1946 – 1951, 2012.

[4] A. Uneri, M. Balicki, J. Handa, P. Gehlbach, R. Taylor, and I. Iordachita, "New steady-hand eye robot with microforce sensing for vitreoretinal surgery research," *Int. Conf. on Biomedical Robotics and Biomechatronics*, pp. 814–819, 2010.

[5] H. Meenink, R. Hendrix, P. Rosielle, M. Steinbuch, and M. de Smet, "A master-slave robot for vitreo-retinal eye surgery," *Proc. of the 10th Int. Conf. of European Society for Precision Engineering and Nanotechnology*, 2010.

[6] S. Charles, H. Das, T. Ohm, C. Boswell, G. Rodriguez, R. Steele, and D. Istrate, "Dexterity-enhanced telerobotic microsurgery," *Proc. of the IEEE Int. Conf on Advanced Robotics*, pp. 5–10, 1997.

[7] W. Wei, R. Goldman, N. Simaan, H. Fine, and S. Chang, "Design and theoretical evaluation of micro-surgical manipulators for orbital manipulation and intraocular dexterity," *ICRA*, pp. 3389–3395, 2007.

[8] M. Nasseri, M. Eder, S. Nair, E. Dean, M. Maier, D. Zapp, C. Lohmann, and A. Knoll, "The introduction of a new robot for assistance in ophthalmic surgery," *35th Annual Int. Conf. of the IEEE Engineering in Medicine and Biology Soc. (EMBC'13)*, 2013.

[9] A. Guerrouad and P. Vidal, "Smos: Stereotaxical microtelemanipulator for ocular surgery.," *Medicine and Biology Society*, pp. 879–880, 1989.

[10] P. Caers, A. Gijbels, M. De Volder, B. Gorissen, P. Stalmans, D. Reynaerts, and E. Vander Poorten, "Precision experiments on a comanipulated robotic system for use in retinal surgery.," vol. Proc. of the 2011 SCATh Joint Workshop on New Technologies for Computer/Robot Assisted Surgery, 2011.

[11] A. Gijbels, N. Wouters, P. Stalmans, H. Van Brussel, D. Reynaerts, and E. Vander Poorten, "Design and realisation of a novel robotic manipulator for retinal surgery," *Proc. IEEE Int. Conf. on Intelligent Robots and Systems (IROS).*, 2013.

[12] M. Charles and N. Brown, "Dimensions of the human eye relevant to radiation protection," *Physics in Medicine and Biology*, vol. 20(2), pp. 202–218, 1975.

[13] G. Zong, X. Pei, J. Yu, and S. Bi, "Classification and type synthesis of 1-dof remote center of motion mechanisms," *Mechanism and Machine Theory*, vol. 43, pp. 1585 – 1595, 2008.